JGR Space Physics

RESEARCH ARTICLE
10.1029/2017JA024930

# Modulation of Electromagnetic Ion Cyclotron Waves by Pc5 ULF Waves and Energetic Ring Current Ions

**Amar Kakad[1], Bharati Kakad[1,2], Yoshiharu Omura[2], Ashwini K. Sinha[1], Aditi Upadhyay[1], and Rahul Rawat[1]**

[1]Indian Institute of Geomagnetism, Navi Mumbai, India, [2]Research Institute for Sustainable Humanosphere, Kyoto University, Kyoto, Japan

**Key Points:**
- Short- and long-period modulations of EMIC waves are observed at Indian Antarctic station Maitri
- Short periodicities are linked with Pc5 waves generated due to field line oscillations, and long periodicities with ring current drifting ions
- Higher sweep rates are associated with stronger EMIC rising tone emissions on ground

**Correspondence to:**
A. Kakad,
amar@iigs.iigm.res.in

**Citation:**
Kakad, A., Kakad, B., Omura, Y., Sinha, A. K., Upadhyay, A., & Rawat, R. (2019). Modulation of electromagnetic ion cyclotron waves by Pc5 ULF waves and energetic ring current ions. *Journal of Geophysical Research: Space Physics*, *124*, 1992–2009. https://doi.org/10.1029/2017JA024930

Received 27 OCT 2017
Accepted 19 FEB 2019
Accepted article online 7 MAR 2019
Published online 30 MAR 2019

**Abstract** We present a ground observation of modulations of strong electromagnetic ion cyclotron (EMIC) waves by short and long periodicities at Indian Antarctic station, Maitri. The signatures of these waves were evident in the magnetic field variations recorded by an induction coil magnetometer during the interval 4.7–7.2 UT on 17 September 2011, a moderately disturbed day. These waves were preceded by a gradual increase in the solar wind dynamic pressure, which started at 3.88 UT. The discrete rising tone EMIC waves were observed in the Pc1 frequency band (~0.5–0.9 Hz). The investigation of the periodicities of the observed wave spectrogram shows the presence of short (≈2.4 min) and long (≈39–69 min) periodicities. Our analysis shows that the short periodicities are associated with the Pc5 Ultra Low Frequency (ULF) waves generated by magnetic field line oscillations, while long periodicities might be associated with the ring current drifting ions. A new method, based on the cross-correlation technique, is adopted to determine sweep rates of the discrete rising tones. The average sweep rates estimated in the range of 0.44–1.9 mHz/s are relatively low as compared to the past reports of sweep rates derived from the satellite observations of EMIC waves. We found that the higher sweep rates are associated with the stronger EMIC waves on the ground, which is in agreement with the theoretical studies. This suggests that the theoretically proposed dependence of sweep rate on strength of EMIC wave in the generation region is retained even during the propagation of these waves to the ground.

## 1. Introduction

In recent years, there have been considerable interest in studying electromagnetic ion cyclotron (EMIC) waves in the inner and the outer magnetosphere through observations, theory, and simulations (Chen et al., 2016; Fraser et al., 2010; Guo et al., 2016; Kubota et al., 2015; Omura & Zhao, 2012, 2013; Remya et al., 2015, 2018; Shoji & Omura, 2011). EMIC waves are excited in the equatorial region of the inner magnetosphere by the ion cyclotron instability of energetic ions with an anisotropic energy distribution. The regimes of the ion cyclotron instability differ at latitudes beyond and near the plasmapause projection. The outer magnetosphere is often marginally unstable for the growth of EMIC waves; thus, even modest compression of the magnetosphere can trigger the excitation of the EMIC waves over a range of L shells (Anderson & Hamilton, 1993; Engebretson et al., 2002). At lower latitudes near the plasmapause, EMIC waves are generated by ring current protons in the late recovery phase of magnetic storms. In both cases, after generation, the EMIC waves propagate along the magnetic field lines to the ionosphere. When the left-hand polarized Pc1 waves enter the high-latitude ionosphere, the interaction with the anisotropic ionospheric plasma results in compressional mode generation. A part of the compressional wave can be trapped in the ionospheric duct at the F-layer and propagate horizontally to lower or higher latitudes. Some of these waves can penetrate into the atmosphere while propagating along magnetic field lines (Johnson & Cheng, 1999; Kim & Johnson, 2016), and they can be observed as Pc1 geomagnetic pulsations in the frequency range of 0.2–5.0 Hz on the ground at high latitudes by induction coil magnetometers (ICMs).

The EMIC waves are mainly seen around both dusk and dawn sectors, with the prevalent occurrence of hydrogen band EMIC waves in the vicinity of dawn sector (Min et al., 2012). Occasionally, these waves are observed in the envelopes of structured rising tone emissions in the ground and the spacecraft ICM data. The ground observations of Pc1/Pc2 waves with a highly structured appearance in the spectrogram were attributed to the bouncing wave packets moving away from the equator and reflecting back from the

ionosphere (Kangas et al., 1998). However, such possibility was challenged by many other observational studies (Fraser et al., 2013; Mursula, 2007). It is believed that the process of structuring and formation of the envelopes of EMIC emissions is linked with the modulation of EMIC waves by various geomagnetic pulsations. The EMIC waves and their modulation by Pc3, Pc4, and Pc5 pulsations have been investigated for a long time with both ground-based instruments and satellite experiments (Demekhov, 2007; Loto'Aniu et al., 2009; Mursula et al., 2001; Rasinkangas & Mursula, 1998, Rasinkangas et al., 1994). The ULF pulsations with the amplitudes of about 4–10 nT and a period of about 250 s correlated with Pc1 activity were detected by CRRES at L ≃ 7 (Rasinkangas et al., 1994). The EMIC wave bursts modulated by magnetospheric Pc3 waves of upstream origin was observed by the Viking satellite inside the magnetosphere (Rasinkangas & Mursula, 1998). The correlation between Pc1 wave packets and Pc3/Pc4 pulsations was seen in the Polar satellite data by Mursula et al. (2001). Loto'Aniu et al. (2009) have reported the frequency/periodicity correlation between Pc1 EMIC wave envelopes and simultaneously observed compressional Pc5 ULF waves using magnetic data measured by the CRRES spacecraft. Although we have gathered sufficient understanding about Pc1/Pc2 EMIC waves, the significance of their source modulation by Pc4/Pc5 waves is yet to be understood well (Menk, 2011).

In this paper, we report the observation of EMIC waves modulated by shorter and relatively longer periodicities recorded at the Indian Antarctic station, Maitri. The Indian Antarctic station Maitri (geographic coordinates, 70.7°S, 11.8°E, and geomagnetic coordinates, 63.1°S, 53.6°E) has been an important location for ground-based observational studies of the geomagnetic processes. Maitri has a unique location; it is outside the auroral oval during geomagnetically quiet times and behaves as a midlatitude station, whereas it lies in the auroral oval during geomagnetically disturbed conditions. The Indian Institute of Geomagnetism conducts several experiments to investigate the geomagnetic processes at Maitri, including an ICM, which has been in operation since 2011. However, so far, the ICM observations have not been examined for studying the EMIC wave activity at Maitri except the recent study of EMIC wave subpacket structures by Kakad et al. (2018). In the present paper, we report the observation of intense EMIC emissions in ground magnetic records at Maitri, which are modulated by shorter and longer periodicities. We have examined the possible mechanism for the observed modulation of EMIC waves.

This paper is organized as follows. In section 2, we describe the experimental setup and data used. Observation of EMIC waves and the interplanetary parameters are discussed in section 3. The periodicities of the EMIC waves are studied in section 4. The method for calculation of the sweep rate is presented in section 5. The present work is discussed in section 6 using the nonlinear theory proposed by Omura et al. (2010) for EMIC waves. Finally, the present work is summarized and concluded in section 7.

## 2. Experimental Setup and Data Usage

We used magnetic field data recorded by the ICM at Maitri. The ICM (LEMI-30i provided by Lviv Centre of Institute for Space Research, Ukraine) comprises of three induction coils and a communication and measuring unit. Two of the induction coils are aligned in geomagnetic north-south and geomagnetic east-west direction, whereas the third induction coil is placed in the vertical direction (Manu et al., 2015). The ICM typically measures variation in magnetic field (i.e., $dB/dt$) at a considerably higher sampling rate (64 Hz) and provides a higher signal-to-noise ratio in the upper ULF range, which includes the Pc1, Pc2, and Pc3 (0.2–45 s) pulsations and the more irregular Pi1 (1–40 s) pulsations. We know that the total magnetic field is given by $B^2 = H^2 + Z^2$, where $H$ and $Z$ are geomagnetic north-south and the vertical component of magnetic field. Thus, the variation in the total magnetic field can be obtained using $\Delta B = (H\Delta H + Z\Delta Z)/B$, where $\Delta H$ and $\Delta Z$ are the variations recorded by ICM in geomagnetic north-south and vertical direction. The values of $H$, $Z$, and $B$ for a given day are obtained using IGRF model. Here we took $H = 19{,}227$ nT, $Z = -41{,}159$ nT, and $B = 45{,}429$ nT. In addition, we used the 1-min resolution data of total magnetic field recorded by proton precession magnetometer (PPM) at Maitri. We have also used the geomagnetic activity indices such as *AU*, *AL*, and *SYM-H* and the interplanetary solar wind parameters such as the magnetic field, speed, density, pressure, and temperature to examine their link to the EMIC wave activity. The electron fluxes in different energy bands, recorded by GOES-13 and GOES-15, were used to explore the impact of wave-particle interaction processes on the population of energetic particles in the inner magnetosphere.

It may be noted that sometimes local geology (crustal conductivity distribution) at the observation station can influence the $Z$ component through crustal currents. Such contributions can influence certain frequency ranges depending on the nature of these crustal currents. We have checked the raw signals from the ICM

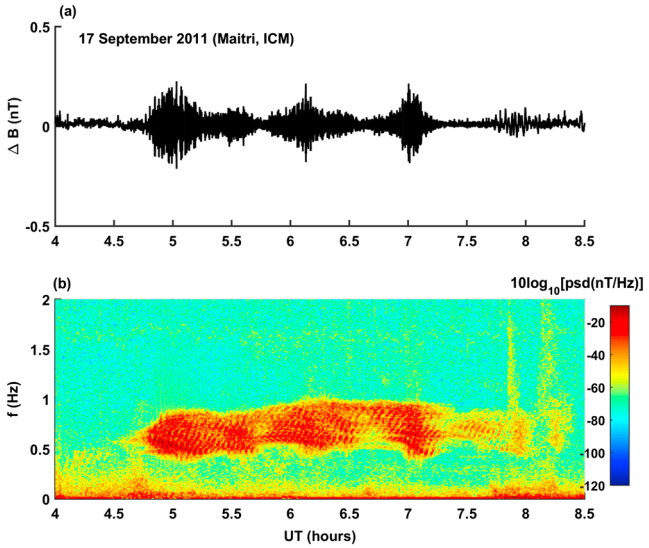


**Figure 1.** (a) Variations in the total magnetic field recorded by the induction coil magnetometer (ICM) at the Indian Antarctic station Maitri ($L = 5$) on 17 September 2011. The sampling rate is 64 Hz. (b) The corresponding spectrogram of these variations in the total magnetic field. Strong electromagnetic ion cyclotron wave activity is observed during 4.7–7.2 UT with distinct electromagnetic ion cyclotron rising tone emissions in the frequency band 0.5–0.9 Hz.

and their Fourier spectra for both $Z$ and $H$ components. They show a peak around 0.5–0.9 Hz (i.e., PC1), which is associated with the EMIC waves. Also, the amplitude of variations in the $Z$ component is relatively small compared with the $H$ component. This suggests that the contribution due to crust inhomogeneities in the $Z$ component is less significant.

In the present study, we have performed the Fourier transform of different signals used in the study. Generally, the signal characteristics and analysis methods both influences the estimates of frequency in the Fourier spectrum (Di Matteo & Villante, 2018). Thus, it is important to test the significance of the observed spectral peaks. Gilman et al. (1963) proposed the method to get the red noise spectrum that can be used in constructing the null hypotheses for statistical significance test. It is given by the following equation:

$$P_h = S_0 \frac{1-\rho^2}{1-2\rho\cos[h\pi/M_{sp}]+\rho^2}. \quad (1)$$

Here $\rho$ is the one lag autocorrelation of original signal that is under testing, and $M_{sp} = N/2$ is the number of samples available in the frequency domain, where $N$ is the length of signal used while performing the Fourier transform. The parameter $h$ is a counter used to incorporate frequency information that varies from 0 to $M_{sp}$. When $\rho = 0$, we get a white noise spectrum. The parameter $S_0$ appears in the equation to make the mean power in the original signal and the red noise spectrum the same (Schulz & Mudelsee, 2002). Then we computed the red noise spectrum with 90% significance level by applying a standard chi-square test such that $P_h^{90\%} = P_h \times \chi^2_{90\%}/dof$. Here the value of $\chi^2_{90\%}$ can be obtained from its statistical table and the degree of freedom $dof \approx N/M_{sp}$. The power spectra shown in the present study are superimposed with their corresponding red-noise spectra having 90% statistical significance.

## 3. EMIC Wave Activity and Interplanetary Parameters

In this section, we discuss the characteristics of EMIC emissions observed at Maitri on 17 September 2011. The variations in total magnetic field recorded by the ground ICM are shown in Figure 1a. The Fourier spectrogram of these variations in total magnetic field recorded by the ICM is shown in Figure 1b. A sliding window of 80 s with an overlap of 90% is used to get the spectrogram. The spectrogram has a resolution of 0.0125 Hz and 8 s in frequency and time domains, respectively. Strong EMIC wave activity is clearly seen around the time interval 4.7–7.2 UT over the frequency range of 0.5–0.9 Hz. It has distinct EMIC rising tone emissions enveloped by the long time period wave. It is seen that the series of small bursts in the magnetic field variations in Figure 1a are associated with the EMIC wave packets shown in Figure 1b. In order to look into the triggering source and modulation for these EMIC waves, we examined the interplanetary solar wind parameters.

It is a moderately disturbed day with midlatitude geomagnetic activity index $Ap = 32$. Figure 2 shows the variation of the solar wind and interplanetary parameters, and the geomagnetic activity indices on 17 September 2011. One-minute resolution interplanetary magnetic field and the solar wind parameters were obtained from the OMNIWEB website. These parameters are time shifted to the Earth's bow shock nose. At around 3.88 UT (4.67 LT), an increase in the total interplanetary magnetic field, solar wind density, solar wind dynamic pressure, solar wind speed, and solar wind temperature is observed (Figures 2a, 2b, 2c, 2e, and 2f, respectively). This time is marked by vertical dashed (red color) lines in Figure 2. The corresponding variations in the high-latitude auroral $AU$ and $AL$ indices are shown in Figures 2d and 2g, respectively. It may be noted that the Maitri station falls in the dawn sector during the initiation of the moderate shock. Although the increase in the above-mentioned parameters was relatively small, it resulted in an increase of approximately 20 nT in SYM-H (Figure 2h). The small pressure pulse (an increase of 1 to 3 nPa at 3.88 UT) was followed by strong EMIC wave activity after about 0.8 hr, and the strong activity lasted for about 2.5 hr (4.7–7.2 UT). The interval of EMIC wave activity is marked by the yellow patch in Figure 2. The EMIC wave

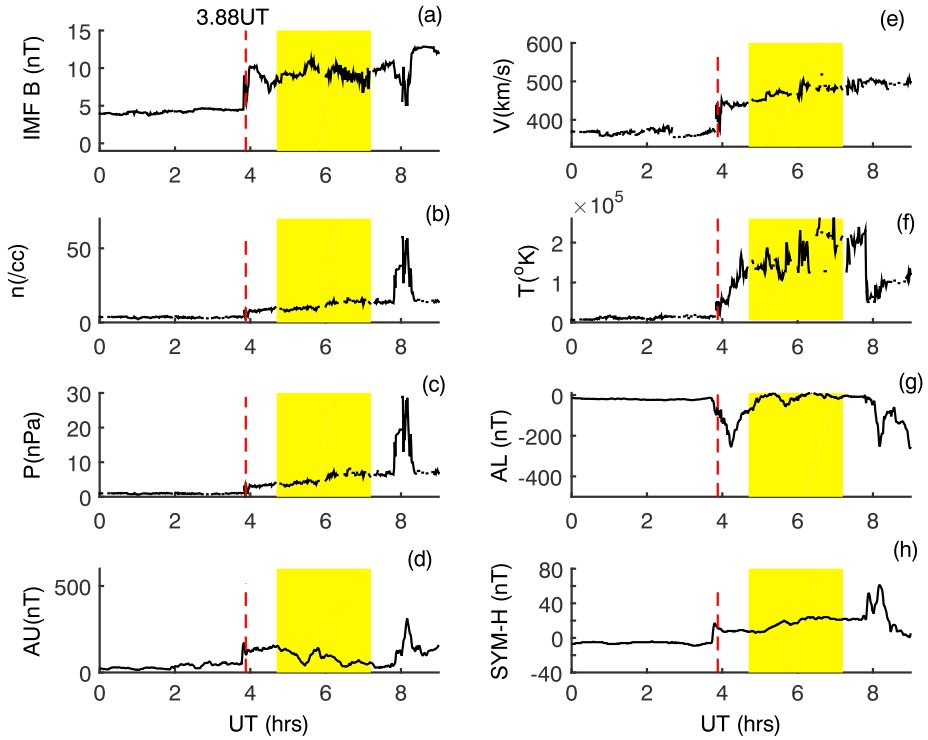


**Figure 2.** Variation of solar wind parameters and interplanetary magnetic field (IMF) on 17 September 2011 ($Ap = 32$) at bow shock nose of Earth's magnetosphere. The time-shifted data were obtained from the OMNIWEB database. The (a) IMF, (b) solar wind plasma density, (c) solar wind dynamic pressure, (d) *AU* index, (e) solar wind flow speed, (f) solar wind plasma temperature, (g) *AL* index, and (h) *SYM-H* index are shown. A moderate interplanetary shock was observed at 3.88 UT at the bow shock nose (shown by the vertical red dotted line). The electromagnetic ion cyclotron wave activity is observed approximately 0.8 hr later. The interval 4.7–7.2 UT of electromagnetic ion cyclotron wave activity is marked by the yellow patch.

activity is observed even after 7.2 UT in the same frequency range. Furthermore, the second enhancement in the solar wind dynamic pressure was initiated at 7.8 UT with 7.8 nPa and reached up to ~30 nPa at 8 UT. Around 7.9 UT, the frequencies of the EMIC waves were also found to be extended to higher frequencies (i.e., 0.5–1.7 Hz) for a short duration. This is an indication that the EMIC wave activity was stimulated for a short interval over a wider range of $L$ shells than was the case for the preceding wave activity (Engebretson et al., 2015). Increase in higher cutoff frequency of the EMIC wave activity suggests that the generation of EMIC waves might have been extended preferably to lower $L$-shells. Earlier studies have reported that EMIC wave occurrence rates in both dawn and dusk sectors peak during geomagnetic storms and substorms and periods of enhanced solar wind dynamic pressure (Erlandson & Ukhorskiy, 2001; Halford et al., 2010; Usanova et al., 2012). Thus, the observed moderate increase in solar wind dynamic pressure can be the source for EMIC wave activity on 17 September 2011.

Another obvious question is related to the EMIC wave band. In the generation region, one can identify the EMIC bands based on the knowledge of local particle gyro-frequencies ($q_s B/m_s$, here s = $H^+$, $He^+$). However, identification of the EMIC wave bands from the ground observations is not straightforward as the information of $L$ shell is not known because of their propagation through the ionospheric duct. Theoretical studies of EMIC waves have demonstrated that the frequency extent of the proton band EMIC emissions is larger than the helium band EMIC emissions (Shoji et al., 2011). In our study, the EMIC wave activity is seen between 0.5 and 0.9 Hz, and the wave has fairly wider frequency extent (~0.4 Hz). Thus, we can speculate that the EMIC wave activity observed on 17 September 2011 is associated with the proton band.

## 4. Periodicities of the EMIC Rising Tone Emissions

We examined the periodicities of these structured waves in the observed EMIC frequency band. The EMIC wave spectrogram shows a lower and upper frequency cutoff at approximately $f_l = 0.5$ Hz and $f_u = 0.9$ Hz,

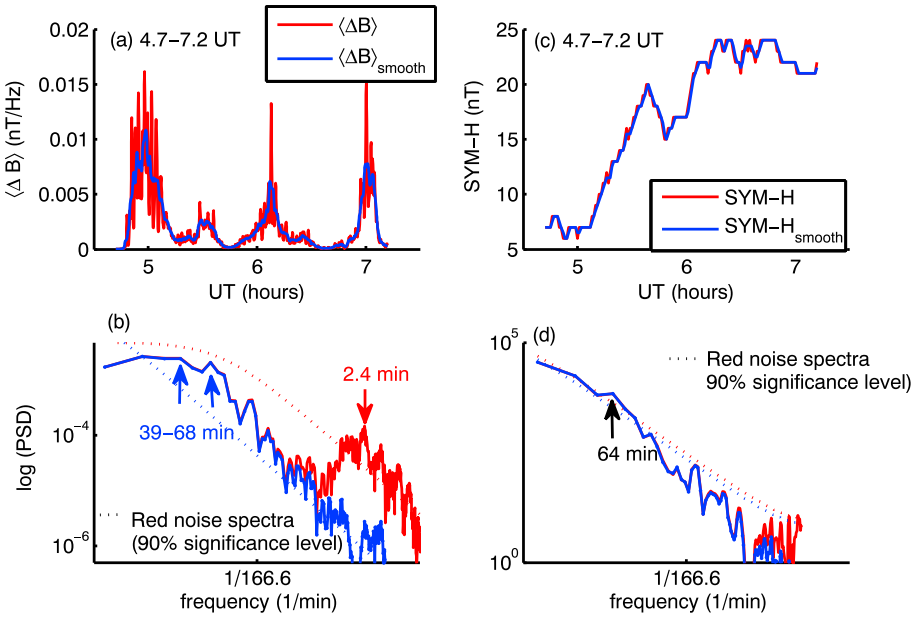


**Figure 3.** (a) The average power in the electromagnetic ion cyclotron (EMIC) wave spectrogram $\langle \Delta B \rangle$ superimposed with its smoothed variations $\langle \Delta B \rangle_{smooth}$ is shown as a function of time. This average power is linked with the EMIC wave spectrogram at frequency 0.5–0.9 Hz. (b) The power spectral density (PSD) obtained by applying Fourier transform to $\langle \Delta B \rangle$ and $\langle \Delta B \rangle_{smooth}$ is shown as function of frequency. Both short (≈2.4 min) and relatively long periodicities (≈39–68 min) are observed in the EMIC rising tones during 4.7 to 7.2 UT. (c) The time variations of *SYM-H* (a measure of ring current) superimposed with its smoothed signal during 4.7–7.2 UT (d) shows the Fourier transform of the *SYM-H* and smoothed *SYM-H* as a function of frequency. The peaks identified in the spectrums are marked with the arrows. The dotted lines in the lower panels represent the red noise spectrum with 90% statistical significance.

respectively. We selected these two frequencies to estimate the average power in the EMIC wave spectrogram. At a given time, the average power is obtained by averaging the power spectral densities associated with EMIC waves from $f_l$ to $f_u$. The time variation of the estimated averaged power $\langle \Delta B \rangle$ is shown in Figure 3a (red color), and it has a time resolution of 8 s. It may be noted that apart from short-period fluctuations, the long-period oscillations (four-peak type structure) are evident in variation of $\langle \Delta B \rangle$. To get the clear signatures of the long-period variations, we smoothed the $\langle \Delta B \rangle$, which is also shown in Figure 3a (blue color). The smoothing is carried out with centered window of approximately 2.8 min. Both these signals are Fourier transformed to determine the dominant periodicities linked with the EMIC waves. We have plotted the Fourier transformed spectrum of both $\langle \Delta B \rangle$ and $\langle \Delta B \rangle_{smooth}$ in Figure 3b as a function of frequency. The dotted lines in Figure 3b represent the red noise spectrum with 90% significance. It may be noted that both Fourier spectra (red and blue) are similar at the lower frequencies (i.e., longer period) and they are different in the higher frequency regime (i.e., shorter period), which is due to the smoothing of the signal. In the EMIC wave, two periodicities are clearly evident with approximate periods of 39–68 and 2.4 min, and they are above 90% of significance level. The short periodicities of few minutes are linked with the repetitive behavior of discrete EMIC rising tones and correspond to Pc5 pulsation periods. Wave observations in the magnetosphere often show simultaneous presence of EMIC waves and longer-period ULF pulsations (Fraser et al., 1992; Mursula et al., 2001). Studies have also suggested a linkage between ULF wave periods and repetition periods of pearl EMIC waves (Mursula et al., 2001). However, the physical mechanism responsible for the modulation of EMIC waves by Pc5 still remains unclear. The long time periods (39–68 min) observed in the current study are longer than those reported earlier (1.7–16.6 min) on the basis of ground and satellite observations (Fraser et al., 1992; Mursula et al., 2001).

First, we made an attempt to identify the mechanism responsible for the observed long-period oscillations in the EMIC event. Singh et al. (2012) determined the approximate drift frequency of ring current ions to

lie in the range of approximately 0.01 to 1.0 mHz. The drift frequency is given by the following equation (Baumjohann & Treumann, 1997):

$$f_d = \frac{3WL\ [0.35 + 0.15\sin(\alpha_{eq})]}{\pi q B_{eq} L^3 R_E^2}, \tag{2}$$

where $W$ is the particle energy in Joules, $R_E$ is the radius of the Earth in meters, $\alpha_{eq}$ is the equatorial pitch angle, and $f_d$ is the drift frequency expressed in Hertz. For $\alpha_{eq} = 0°$ and $\alpha_{eq} = 90°$ this expression reduces to $8.2343W/[B_{eq}L^2]$ and $11.7633W/[B_{eq}L^2]$, respectively, where $W$ and $B_{eq}$ are expressed in MeV and nT, respectively. Here $B_{eq}$ is the ambient equatorial magnetic field at L-shell. We used the Tsyganenko model to estimate the ambient magnetic field ($B_{eq}$) in the vicinity of the equatorial crossing of the magnetic field lines having $L = 5$, 6, and 7. For the interplanetary conditions at 3.88 UT on 17 September 2011, the model gives the magnetic field $B_{eq}$ as 274, 171, and 122 nT, respectively, at these L shells. In the equatorial region, the pitch angle of ions is larger, and it shows peak close to 90° (Chen et al., 1999). By taking $\alpha_{eq} = 90°$, if we substitute these values of L-shell and corresponding ambient magnetic fields in equation (2), we obtain the drift period $\tau_d$ in minutes as $10.8/W$, $9.7/W$, and $9.4/W$, respectively, for $L = 5$, 6, and 7. Here we speculate that the long period (39–68 min) modulation of EMIC waves are associated with the ring current particles. The hot proton density plays a key role in the generation of EMIC waves, and drifting ring current particles can significantly influence the hot proton density in the source region. By assuming this possibility to be true, we need protons of energies 123–248 keV to produce these long-period oscillations of 39–69 minutes. Now the question arises whether we have protons of these energies in the ring current region to support this argument. We do not have any direct observation of proton flux in the ring current region for this event. Based on the earlier and recent studies, however, we argue that the presence of 123–248 keV cannot be completely dismissed. In the ring current region, the dominance of different ions in various energy regimes depends on the level of geomagnetic activity. Tetrick et al. (2017) examined the proton flux during different magnetic storms and found that the ring current proton flux is mainly associated with 5–70 keV. Daglis et al. (1999) have shown that the ion energies are relatively higher during the quiet time as compared to magnetically disturbed periods. Their study suggests the presence of 100- to 200-keV protons. A statistical study by Zhao et al. (2015) suggests the difference in the proton energies during prestorm, storm, and poststorm periods. The EMIC wave event in Figure 1 is observed during the sudden commencement phase of the moderate geomagnetic storm. Therefore, we may consider relatively higher energies (>70 keV) for the resonant protons. A recent study using Van Allen Probes reported that the ring current proton flux with energies ranging from 50 keV up to several hundred keV is the dominant component of plasma pressure during both quiet and active periods (Yue et al., 2018). The energy of ring current protons needed to produce the speculated long-period modulation of EMIC waves is marginally higher (123–248 keV) than the energies reported in recent studies (70 to several hundred keV). Thus, we speculate that long period oscillations enveloping the EMIC emissions might be associated with the drifting ring current particles.

Second, we explore the possible source for the short periodicity seen in the EMIC waves (≈2.4 min). A sudden change in solar wind dynamic pressure causes oscillations in surface currents at the magnetopause boundary for nullifying the imbalance in the pressure. These oscillations in the current cause compressional oscillations in the magnetic field in the magnetosphere, which can locally excite field line oscillations at selected $L$ values (Baumjohann et al., 1984). The field line resonance in the magnetosphere is almost simultaneously excited with the passing of the wave front of the initial impulse (Fujita et al., 2001). The field line response to the oscillating currents at the magnetopause boundary caused by sudden change in solar wind dynamic pressure is most dominant in the dawn and dusk sector (Sinha & Rajaram, 2003). A statistical study by Zhang et al. (2010) suggests that the poloidal and toroidal ULF waves excited by positive and negative pressure pulses are stronger around local noon than those in the dawn and dusk sectors. The field line oscillation can be a likely source for these short (Pc5) periodicities because such oscillations can modify the gradient of the magnetic field in the generation region of EMIC waves. Generally, the field line oscillations can be seen along the magnetic field line and even at its footprint on the ground, that is, at Maitri.

So far, we have only discussed the mechanisms as possible sources for the short (≈2.4 min) and long (≈39–68 min) periods seen in the EMIC wave event. However, to support this hypothesis, one has to demonstrate the presence of these periods in the *SYM-H*, a measure of the ring current and total magnetic field recorded at Maitri during the EMIC wave period (4.7–7.2 UT). For this purpose, we took *SYM-H* data from

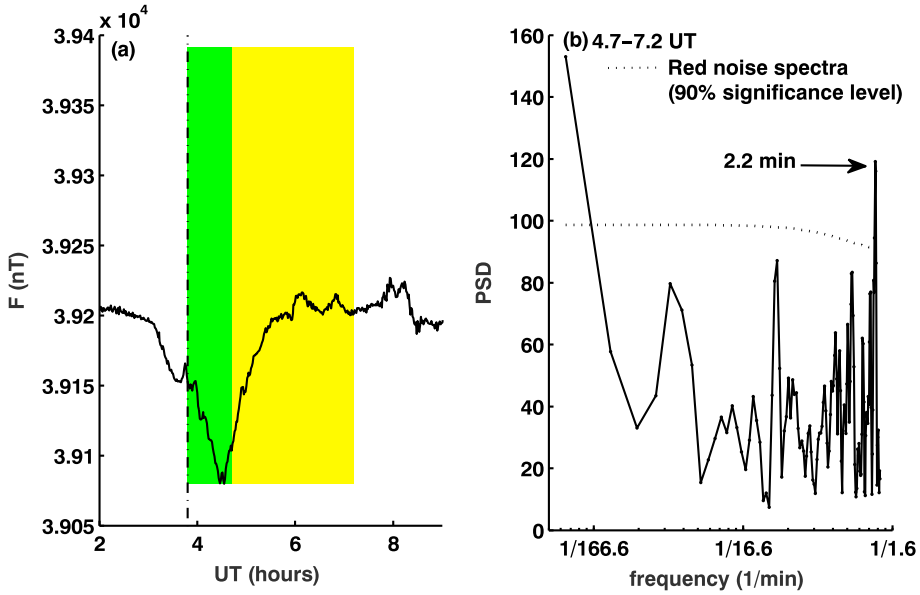


**Figure 4.** Time variation of (a) total magnetic field recorded by proton precession magnetometer at Maitri. The sampling rate is 1 min. The vertical black dotted line indicates the time of initiation of the moderate shock at 3.88 UT, and the yellow patch represents the duration of electromagnetic ion cyclotron wave activity. The green patch shows the time interval between initiation of the moderate shock and the start of electromagnetic ion cyclotron wave activity. (b) The power spectral density (PSD) is shown as a function of frequency obtained from the Fourier transform of the magnetic field variations at Maitri during the interval marked by the yellow patch. The dotted lines in the right-side panel represent the red noise spectrum with 90% statistical significance. The signature of field line oscillations having periods close to 2.2 min (Pc5) is clearly evident in the power spectrum.

WDC Kyoto, and total magnetic field data recorded by PPM at Maitri. These data sets are of 1-min resolution. We are interested in gathering information of short periodicities in PPM data and long periodicities in *SYM-H* data. While using Fourier analysis on these observations, we applied 3-point smoothing to *SYM-H* data to remove short periods. On the other hand, while using PPM data we removed 3-point smoothed signal from the observation to obtain the short-period variations. This is nothing but the low-pass and high-pass filtering of the original signals. In Figure 3c we have shown both *SYM-H* and smoothed *SYM-H* index, and their respective Fourier spectrums are presented in Figure 3d. The dotted lines indicate the red noise spectrum with 90% significance. It is noted that the behavior of original and smoothed *SYM-H* spectrum are the same. But there is a difference in the spectrum in the higher frequency regime, which is expected because of the smoothing. It suggests that the 3-point smoothing applied to the *SYM-H* signal does not modify/suppress the frequency information in the lower frequency domain. The spectral power shows the peak corresponding to 64 min, and it is above 90% significance level. This period is close to the long periodicities observed during the EMIC wave activity. It suggests that the relatively long period (39–68 min) modulation observed in the EMIC waves can be related to the ring current particle drift motions. In earlier study it is shown that the signature of the westward modes associated with the westward drift of ring current proton can be seen on global scale (Singh et al., 2012) and these modes can be identified using the ground-based magnetometer data.

The observations of total magnetic field recorded at Maitri are shown in Figure 4a. Here green patch (3.8–4.7 UT) indicates the interval after the enhancement in kinetic pressure, whereas the yellow patch indicates the EMIC wave activity (4.7–7.2). The vertical dashed line indicates the start time for the moderate shock, and the green patch shows the time difference between initiation of the moderate shock and the EMIC wave activity. The Fourier spectrum of the total magnetic field recorded by PPM is carried out for the interval marked by the yellow patch, which is shown in Figure 4b. Additionally, the red noise spectrum with 90% significance is plotted with the dotted line in the Figure 4b. It clearly shows the presence of periodicity close to 2.2 min, and it is above the 90% significance. The signature of field line oscillations with few minutes periodicity is found to be present in the ground magnetic field observations. Both mechanisms proposed here could be the possible source for the short- and the long-period modulations observed

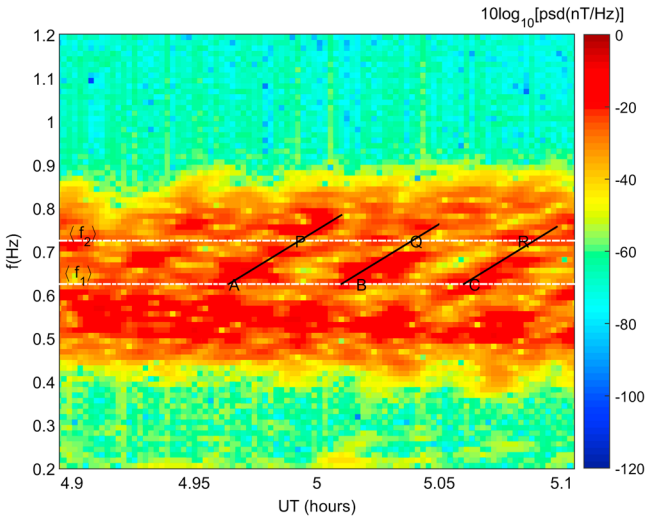


**Figure 5.** (a) Example of a sweep rate computation for a 12-min period between 4.9 and 5.1 UT in the observed electromagnetic ion cyclotron frequency band. Horizontal dashed-dotted line represents the average frequency $f_1 = 0.625$ Hz and $f_2 = 0.725$ Hz. The average power in the electromagnetic ion cyclotron wave spectrogram associated with these frequencies are subjected to cross-correlation technique to estimate the time lag. Points A, B, and C for frequency $f_1$ and P, Q, and R for frequency $f_2$ are marked with reference to the cross-correlation technique (refer Figure 6). A slanted line drawn in the plot indicate the average sweep rate ($S_{rate} = 0.9615$ mHz/s) for this 12-min interval.

in the EMIC wave activity on 17 September 2011. This aspect is further discussed in the section 7 using the nonlinear theory of EMIC emissions.

## 5. Computation of Sweep Rate of the EMIC wave Rising Tone Emissions

We computed the sweep rates of the discrete EMIC rising tones in the observed EMIC band. For a given EMIC discrete emission, a sweep rate is defined as the rate of change of frequency in a given time interval. Generally, one can select two frequencies and their corresponding time in the EMIC wave spectrogram to estimate the sweep rate. However, it is a manual way for the computation of sweep rates. Here we have adopted a new method to compute the sweep rate, which is based on the cross-correlation technique. The cross-correlation between two signals, namely, $x(t)$ and $h(t)$, is given by

$$f(\tau) = \int_{-\infty}^{+\infty} x(t) * h(t+\tau)dt, \tag{3}$$

where $\tau$ is time lag. Using cross-correlation technique, one can find the similarities between two signals at a delayed time, and it is widely used in various studies to obtain time lags between two signals (Briggs, 1984; Engavale et al., 2005). For this, we divided the EMIC wave period 4.7–7.2 UT into 12-min intervals. For each interval, the spectral power corresponding to two frequencies, namely, $f_1$ and $f_2$, was obtained by averaging the EMIC wave spectrogram power from $f_j - 0.05$ to $f_j + 0.05$ Hz, where $j = 1$ and 2. We get two signals corresponding to $f_1$ and $f_2$. As an example, a spectrogram over the 12-min window, starting from 4.90 to 5.10 UT, is shown in Figure 5. The horizontal dashed-dotted lines indicate the two frequencies, $f_1 = 0.625$, and $f_2 = 0.725$, considered for this computation. The corresponding variations of signals at these frequencies are shown in Figures 6a and 6b, respectively. We have marked points $A$, $B$, and $C$ for $f_1$ and $P$, $Q$, and $R$ for $f_2$ in Figures 5, 6a, and 6b. The points $A$, $B$, and $C$ lie on three discrete EMIC emissions at frequency $f_1$, and if we trace these EMIC rising tones at higher frequency $f_2$, then they will be located at points $P$, $Q$, and $R$, respectively. Now these two-time varying signals are subjected to the cross-correlation analysis to compute the time lag ($\tau$) between the signals. The autocorrelation and cross-correlation functions are depicted in Figure 6c as a function of time lag. The autocorrelation function peaks at a time lag $\tau = 0$ as expected, whereas the cross-correlation function has a maximum correlation of 0.75 at time lag $\tau_{m1} = 104$ s. After estimating the time lag, the sweep rate can be estimated using $S_1 = (f_2 - f_1)/\tau_{m1}$. The estimated sweep rate ($S_1$) comes out to be is 0.9615 mHz/s. The slanted lines marked in Figure 5 indicate the sweep rates computed in this 12-min window.

For this 12-min window, we have performed the same analysis by taking two other frequencies, namely, $f_3$ and $f_4$. The corresponding variations of signals at these frequencies are shown in Figures 6d and 6e, respectively, and their autocorrelation and cross-correlation functions are depicted in Figure 6f. When we used these two frequencies, the cross-correlation attains the peak of 0.65 at a time lag of $\tau_{m2} = 96$ s, which gives a sweep rate of $S_2 = 1.04$ mHz/s. By choosing two different pairs of frequencies, that is, ($f_1$, $f_2$) and ($f_3$, $f_4$), for computation of the sweep rate, one can reduce the uncertainty in the estimated average sweep rate defined as $S_{rate} = (S_1 + S_2)/2$. The calculated sweep rates of the EMIC rising tones in our case are in the range of 0.44–1.9 mHz/s, which are smaller than those previously reported (0.1 Hz/s) in the radiation belts (Sakaguchi et al., 2013). By using ground observation of EMIC waves from Athabasca, Canada (magnetic latitude 61.7°N), the sweep rates of few tens mHz/s were reported (Nomura et al., 2016). The cluster satellite observed the EMIC wave with sweep rate 25 mHz/s in the inner magnetosphere (Omura et al., 2010; Pickett et al., 2010).

In this way, for each 12-min interval, we estimated the (i) sweep rate and (ii) integrated power associated with the EMIC wave for the frequency band 0.5–0.9 Hz. In Figure 7a, the variation of the average sweep rate $S_{rate}$ (blue filled circles), sweep rate $S_1$ (blue asterisk) estimated using ($f_1$, $f_2$), sweep rate $S_2$ (blue dots) estimated using ($f_3$, $f_4$), and integrated spectral power (red) of the rising tone emissions is shown as a function

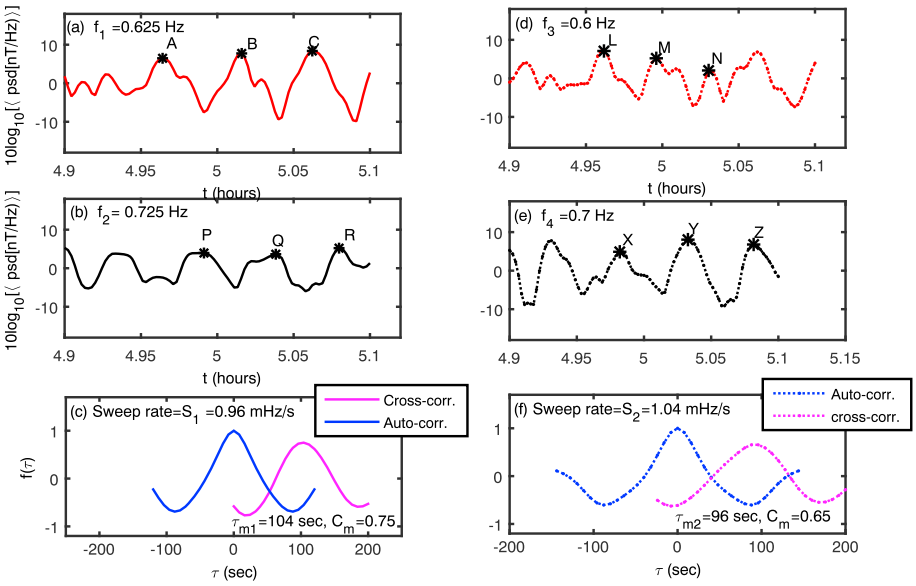


**Figure 6.** The average power in the electromagnetic ion cyclotron (EMIC) wave spectrogram associated with frequencies (a)$f_1 = 0.625$ Hz and (b)$f_2 = 0.725$ Hz. Points A, B, and C are associated with $f_1$ for three distinct EMIC rising tone emissions, which can be seen at points P, Q, and R at later time corresponding to frequency $f_2$, and (c) their autocorrelation (blue) and cross-correlation (magenta) as functions of time lag $\tau$. The maximum cross-correlation is 0.75 at a time lag of 104 s. The average power in the EMIC wave spectrogram associated with frequencies (d)$f_3 = 0.6$ Hz and (e)$f_4 = 0.7$ Hz, and (f) their auto-correlation (blue dotted) and cross-correlation (magenta dotted) as functions of time lag $\tau$. The maximum cross-correlation is 0.65 at a time lag of 96 s.

of time. In Figure 7b average sweep rates are plotted as a function of integrated spectral power ($\sum \Delta B$). It is evident that the sweep rate varies with time and the higher sweep rates are associated with the stronger EMIC emissions. However, there is 1 point with larger $\sum \Delta B$ (separated by a vertical dotted line in Figure 7b), which does not follow this tendency. Based on other 14 points, we obtained a correlation coefficient of 0.71, and it is statistically within the 99% significance level. If we include all the points while estimating the correlation, then it comes out to be 0.48, which is within the 90% of significance level.

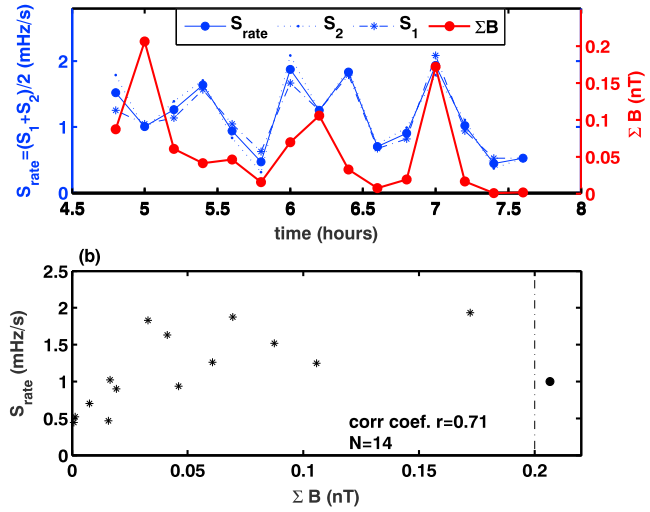


**Figure 7.** For each 12-min interval (a) the average power of the rising tone emissions for the electromagnetic ion cyclotron band (red curve) and the corresponding sweep rate (blue filled circles) are shown as a function of time. The sweep rate $S_1$ ($S_2$) obtained from frequencies $f_1$ and $f_2$ ($f_3$ and $f_4$) is depicted using blue dots (blue asterisk); (b) the estimated average sweep rates ($S_{rate} = 0.5(S_1 + S_2)$) are plotted as a function of integrated power ($\Sigma B$) associated with the EMIC wave. $S_{rate}$ has tendency to increase with $\Sigma B$, and correlation coefficient between them is found to be $r = 0.71$ with an outlier $\Sigma B > 0.2$ nT. By including this outlier point the correlation coefficient decreases to 0.48.

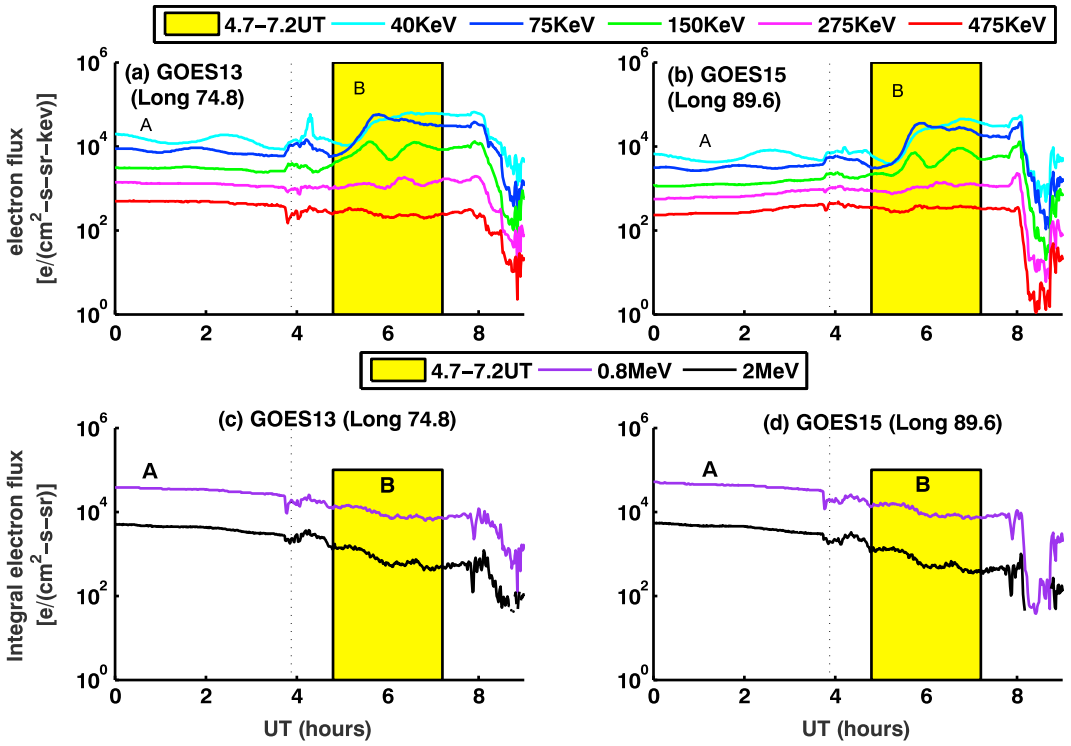


**Figure 8.** Electron flux and integral electron flux observations from GOES-13 (74.8°E) and GOES-15 (89.6°E) at $L = 6.6$. Panels (a) and (b) show the electron flux in the range of 40–475 keV, and panels (c) and (d) show the integral electron flux in the range of 0.8–2 MeV. The yellow patch in the figure marks the electromagnetic ion cyclotron wave activity interval. In each panel points A and B, respectively, represent the time intervals before and during the electromagnetic ion cyclotron wave activity. The vertical dotted line indicates the time of start of moderate shock. The absolute rate of decrease in integral electron flux during interval B is found to be higher as compared with interval A.

The nonlinear theory proposed by Omura et al. (2010) indicates that the sweep rate of EMIC rising tone emission is dependent on the wave amplitude (refer equation (3) in section 7). When an EMIC wave propagates from generation region to high latitude along magnetic field lines, one expects the changes in their characteristics. However, in the frequency domain, the wave information is less altered. In such scenario, the EMIC waves seen on the ground shall follow the same dependence as in the source region. Here we have examined this possibility by estimating the sweep rates and integrated spectral power for an interval of 12 min. We find that the integrated wave power of EMIC emissions is relatively higher when the sweep rates are higher. This association is consistent with the theory of EMIC waves (Omura et al., 2010) in the generation region. It may be noted that the theoretically proposed interrelation of sweep rate and EMIC wave strength is less significantly affected during propagation of EMIC waves to the ground.

When EMIC rising tone emissions are recorded in the ground ICM, it means that the EMIC wave activity has been triggered at some $L$-shell in the generation region ($\pm 10°$ magnetic latitude). Such EMIC rising tone emissions are generated through the highly nonlinear mechanism in the generation region. What we see on the ground is the manifestation of the nonlinear process occurring in the source region, which is often seen as the triggered emissions in the satellite observation. The triggering process needs a constant frequency ion-cyclotron wave with a sufficient amplitude called as threshold amplitude (Omura et al., 2010). After their generation, they propagate along the magnetic field line toward higher latitudes (Kim & Johnson, 2016). When these waves arrive at the footprint in the ionosphere, their signatures can be captured by ground ICMs. An example of simultaneous observation by satellite (showing triggered EMIC waves) and ground ICM (showing pearl type rising tone emission) is reported by Nakamura et al. (2014). In general, the theory discussed in the section 7 is applicable to EMIC rising tone emissions occurring in both proton and helium bands.

**Table 1**
*Absolute Decrease in the Integral Electron Flux Prior to (i.e., Interval A) and During (i.e., Interval B) the EMIC Wave Activity for Two Different Energy Ranges*

| Satellite | Integral electron flux | >0.8 MeV | Integral electron flux | >2 MeV |
|---|---|---|---|---|
| | A (0–3 UT) | B (3.88–7.2 UT) | A (0–3 UT) | B (3.88–7.2 UT) |
| GOES 13 | −3,080 | −4,219 | −520 | −793 |
| GOES 15 | −4,152 | −4,801 | −584 | −702 |

*Note.* The integral electron flux are expressed in unit of e/(cm$^2$.s.sr).

## 6. Particle Loss During EMIC Wave Activity

It is known that the EMIC waves can scatter electrons (Lorentzen et al., 2000; Meredith et al., 2003; Summers & Ma, 2000; Summers & Thorne, 2003) and protons (Sakaguchi et al., 2007; Sandanger et al., 2007; Usanova et al., 2010; Yahnina & Yahnin, 2014; Yahnin et al., 2009) into the atmospheric loss cone. Especially, coherent EMIC rising tone emissions can cause efficient precipitation of relativistic electrons (Kubota et al., 2015; Omura & Zhao, 2012, 2013). To obtain a comprehensive picture of the role of EMIC emissions in particle precipitation, we examined the ground observations at Maitri in conjunction with the energetic electron observations from GOES-13 (74.8°E) and GOES-15 (89.6°E). Observations of 0.8- to 2-MeV electrons are taken from the Energetic Proton Electron and Alpha Detector instrument on GOES-13 and GOES-15, which gives the integral electron flux, and they are expressed in the units of e/(cm$^2$.s.sr). On the other hand, observations of 40- to 475-keV electrons are obtained from the Energetic Particle Sensor-Magnetospheric Electron Detector instrument on GOES-13 and GOES-15, which gives the electron flux and they are measured in the units of e/(cm$^2$.s.sr.kev). Figures 8a and 8b show the variation of the electron flux in five energy bands in the energy range 40–475 keV, observed by GOES-13 and GOES-15 on 17 September 2011, respectively. These five energy bands, respectively, correspond to electrons having energies in the range 30–50, 50–100, 100–200, 200–250, and 350–600 keV (Boynton et al., 2016). In addition, the integral electron fluxes with energies greater than 0.8 and 2 MeV (observed by GOES-13 and GOES-15, respectively) are shown in Figures 8c and 8d, respectively. The start time of moderate shock is marked by vertical dotted lines in Figure 8. The yellow patch represents the EMIC wave activity period (i.e., 4.7–7.2 UT), and it is marked by letter "B" in Figure 8, whereas interval prior to the initiation of moderate shock (i.e., 0–3.88 UT) is marked by letter "A." It is noticed that the integral electron flux in the MeV range decreased during the period of EMIC wave activity. In order to quantify the change in integral electron flux, we estimated their rate of decrease during EMIC wave activity (interval B) and prior to the EMIC wave activity (interval A) for the integral energy fluxes greater than 0.8 and 2 MeV. These rates are summarized in Table 1. It is found that the absolute decrease of integral electron flux prior to the EMIC wave activity is smaller as compared to that during the EMIC wave activity.

Notably, GOES-13 and GOES-15 are located in the longitudinal belt between 74.8° and 89.6° at the geostationary orbit ($L \sim 6.6$). For a given energy and pitch angle, electrons and ions orbit the Earth with approximately the same velocity. As MeV electrons travel faster in the longitudinal direction (~12–13.8 min/rotation at $L = 5$–7), the decrease in their number due to EMIC wave activity can manifest promptly at any longitudinal belt. Further, such a decrease is not seen for electron fluxes in the energy range of 40–475 keV (Figures 8a and 8b). It is believed that the keV-range electrons are generally precipitated by very low frequency (VLF) waves or chorus emissions (Behera et al., 2016, 2017). A large decrease in the flux of these electrons between 8.5 and 10 UT was seen by both GOES-13 and GOES-15, and this decrease might be linked to VLF/chorus wave activity. We have not investigated this possibility because of the unavailability of VLF observations for Maitri.

We examined the Fourier spectra of filtered GOES integral electron fluxes in two different energy ranges, (i) >0.8 MeV and (ii) >2 MeV. As discussed earlier, to obtain the filtered signal, we removed the 3-point smoothed variation of integral electron flux from their corresponding original observation, which is similar to applying the high pass filter. The power spectral densities obtained from the Fourier transform of this filtered Integral electron flux are presented in Figure 9. The dotted lines in each subplot of Figure 9 indicate

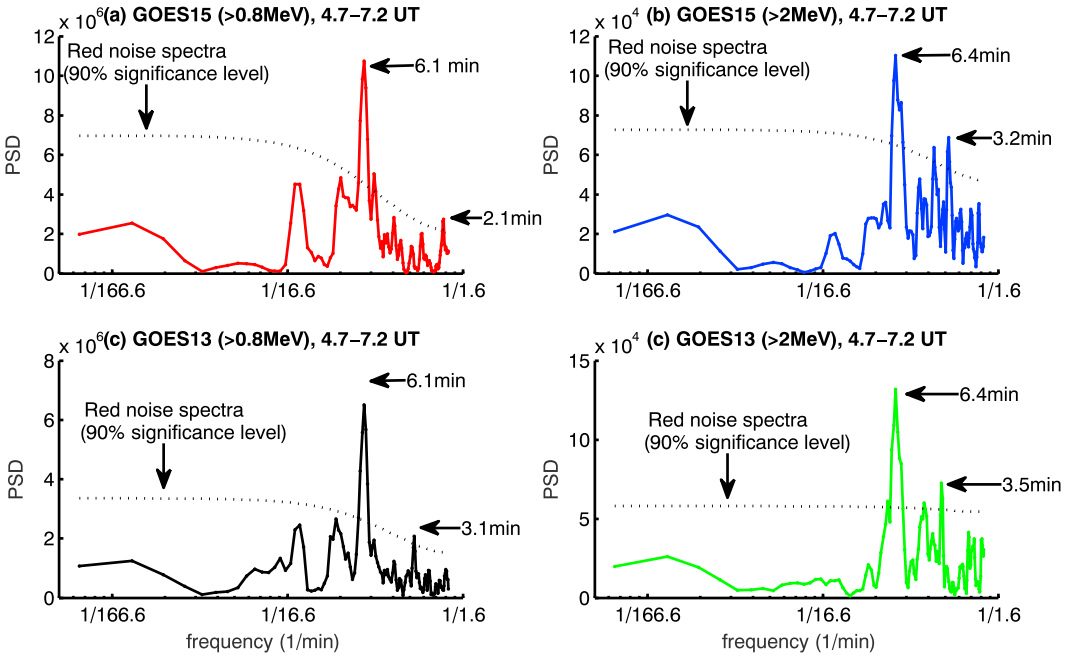


**Figure 9.** The Fourier spectrum of integral electron flux (a) >0.8 MeV, GOES-13 (b) >0.8 MeV, GOES-15 (c) >2 MeV, GOES-13 (d) >2 MeV, and GOES-15 observed on 17 September 2011 during 4.7–7.2 UT is plotted as a function of frequency. The dotted lines in each subplot represent the red noise spectrum with 90% statistical significance.

the red noise spectrum with 90% significance. The period of 3.2–3.5 min is clearly visible for higher energy integral electron flux (>2 MeV), whereas for lower energy integral electron flux (>0.8 MeV), these periods are found to be suppressed. Apart from this, additional 6.5-min periodicity is also evident in the integral electron flux spectra for both integral electron fluxes recorded by GOES-13 and GOES-15. The periodicities of 3.2–3.5 min observed in the integral electron fluxes (>0.8 MeV) could be linked with the EMIC wave activity.

## 7. Discussion

We have noticed two dominant periodicities in the EMIC waves, (i) short period ≈2.4 min, which corresponds to ultra low frequency (6.9 mHz) Pc5 pulsations and (ii) long-period oscillations encompassing the EMIC emissions in the range of 39–68 min (i.e., frequency <0.4 mHz). In order to reconfirm the presence of these short and long time scale periods, we have computed the spectral coherence $c(f)$, which is a measure of correlation between two signals in the frequency domain. The spectral coherence is defined as the ratio of magnitude square of cross-spectral density between two signals $x(t)$ and $y(t)$, that is, $|G_{xy}(f)|^2$ to the product of autospectral density of individual signals, that is, $G_{xx}(f) \times G_{yy}(f)$. We used widely adopted Welch method (Welch, 1967) to get $c(f)$. In this method the original signal is divided into $n_s$ segments of length $T$, with overlapping. For each segment $\tilde{G}_{xy}$, $\tilde{G}_{xx}$, and $\tilde{G}_{yy}$ are estimated, and then spectral coherence is calculated using the following equation:

$$c(f) = |\langle \tilde{G}_{xy} \rangle|^2 / [\langle \tilde{G}_{xx} \rangle \times \langle \tilde{G}_{yx} \rangle]. \quad (4)$$

Here $\langle\rangle$ indicates the ensemble average of the parameter for $n_s$ segments. If we consider a single segment, then the coherence will be always one for all frequencies. It may be noted that the error in the estimated coherence is inversely proportional to the $\sqrt{n_s}$. Thus, we need larger $n_s$ for the reliable estimates of coherence. At the same time, we also require larger $T$ to have good spectral resolution. In such situation, the frequency information in the lower frequency domain can get affected due to chopping of the original signal into a smaller segments of length $T$. In this way, we estimated the spectral coherence, which is shown as a function of frequency in Figure 10 for (a) ICM total variation in B and GOES integral electron flux (>0.8 and >2 MeV), (b) ICM total variation in B and PPM total magnetic field F, and (c) ICM total variation in B and *SYM-H*. The 90% statistical significance level for $c(f)$ is shown by horizontal dotted line in each panel.

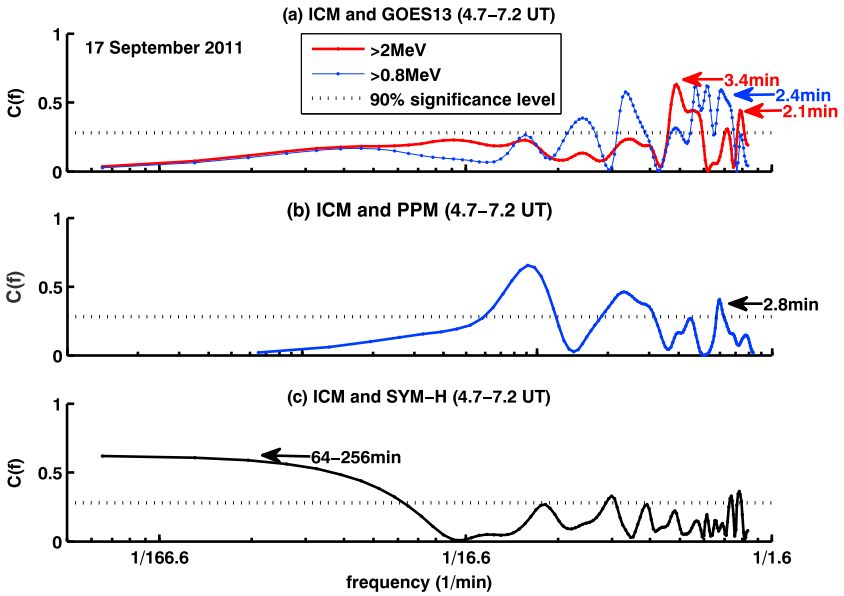


**Figure 10.** The spectral coherence $C(f)$ is shown as a function of frequency for (a) induction coil magnetometer (ICM) and GOES-13 integral electron flux (0.8 > MeV, 2 > MeV), (b) ICM and proton precession magnetometer (PPM) total magnetic field $F$, and (c) ICM and *SYM-H*. The horizontal dotted line in each subplot represents the 90% significance for the spectral coherence, which comes out to be 0.28.

In the spectral coherence the periods of approximately 64–128 and 2.1–3.4 min are clearly evident. It may be noted that in Figure 10c a broad peak is seen at lower frequencies rather than a peak at any particular frequency. But sufficient coherence exists for the periods of 64–256 min. The presence of long and short periods in different data sets during EMIC wave activity is confirmed through the spectral coherence analysis.

Another feature is that the sweep rate and strength of the EMIC wave are positively correlated on the ground. This dependence can be understood using the nonlinear theory of EMIC waves given by Omura et al. (2010). In this theory, the Earth's dipolar magnetic field is approximated by the parabolic equation described as $\Omega_H = \Omega_{H0}(1 + ah^2)$, where, $\Omega_H = qB/m_H$ is the proton gyrofrequency at position $h$ along the magnetic field line and $\Omega_{H0}$ is the proton gyrofrequency at the magnetic equator (i.e., $h = 0$). Here $a = a_0$ corresponds to a dipole magnetic field, $a > a_0$ indicate a magnetic field stretched from the dipole field, and $a < a_0$ gives a compressed magnetic field, where, $a_0 = 4.5/(LR_E)^2$ (Shoji & Omura, 2014).

Equation (40) of Omura et al. (2010) suggests that the inhomogeneity factor $S$ plays an important role in the dynamics of self-sustaining rising tone EMIC emissions. It is a dimensionless quantity. The inhomogeneity factor is crucial, as it determines whether the second-order resonance condition for the nonlinear trapping of a proton (i.e., $v_{\|} = V_R$) is satisfied or not. Here $v_{\|}$ is the parallel velocity of the proton, and $V_R = (\omega - \Omega_H)/k$ is the resonance velocity.

It may be noted that frequency sweep rate $\frac{\partial\omega}{\partial t}$, magnetic field gradient $\frac{\partial\Omega_H}{\partial h}$, and wave amplitude $B_{\mathrm{w}}$ contribute to the factor $S$, which is generally considered in the range of 0.4–0.5 as the maximum resonant current is realized for these values. In the equatorial region, the magnetic field gradient is zero, which yields the following relation (Omura et al., 2010):

$$\frac{\partial\omega}{\partial t} = \frac{0.4\omega s_0}{s_1}\left[\frac{qB_{\mathrm{w0}}}{m_H}\right], \tag{5}$$

The above equation gives the relation between the frequency sweep rate and the wave amplitude in the generation region. Here $B_{\mathrm{w0}}$ is the initial wave amplitude of the EMIC wave. It may be noted that in the generation region, $\partial\omega/\partial t$ is proportional to the initial wave amplitude $B_{\mathrm{w0}}$. We find that this dependence is observed even in the ground observations of EMIC waves. It indicates that this characteristic is retained during their propagation to the ground.

We have noted two periodicities, short (≈2.4 min) and long (≈39–68 min), which are responsible for the modulation of EMIC wave activity at Maitri on 17 September 2011. The mechanism responsible for these

modulations should imprint their signatures in the source/generation region. Here we propose that the field line oscillations and ring current drifting ions as possible sources, respectively, for the short and long periodicities that are seen in the EMIC waves. The nonlinear growth rate equation of EMIC wave is as follows (Omura et al., 2010):

$$\Gamma_{NL} = \omega_{ph}^2 \frac{Q}{2} \left(\frac{V_P}{c\Omega_w \omega}\right)^{1/2} \frac{V_g}{V_{t\|}} \left(\frac{V_{\perp 0}}{c\pi}\right)^{3/2} \exp\left[-\frac{V_R^2}{2V_{t\|}^2}\right]. \quad (6)$$

In the equation above, one can see that the nonlinear growth rate ($\Gamma_{NL}$) of the EMIC wave is controlled by the hot proton density $n_H$ and hot proton temperature anisotropy, that is, $v_\perp/v_\|$. The thermal velocity of the proton in the perpendicular direction is assumed to be equal to their drift velocity, that is, $v_\perp = V_{\perp 0}$. In order to have self-sustaining rising tone emission (i.e., $\partial B_w/\partial t$), the following condition must be satisfied by the wave propagating in a positive direction ($V_g > 0$).

$$\frac{\partial \Omega_w}{\partial h} < \frac{\Gamma_{NL}}{V_g} \Omega_w \quad (7)$$

When the wave is propagating away from the generation region, the gradient in the magnetic field contributes substantially to the factor $S$ as compared to the frequency sweep rate. By rearranging the terms in the expression of the factor $S$, one can obtain the partial spatial derivative of $\Omega_w$. Substitution of this values in the above equation (5), we obtain the following condition for the threshold amplitude of the EMIC wave required for generation of the self-sustaining rising tone emission.

$$\Omega_w > \Omega_{\text{threshold}} = \frac{5 V_P a s_2 \Omega_{H0} V_g}{s_0 \omega \Gamma_{NL}} \quad (8)$$

Equation (6) gives theoretical estimate of the threshold wave amplitude required for the nonlinear wave growth. It may be noted that this threshold wave amplitude is smaller for smaller magnetic field gradient. For the nonlinear growth of EMIC rising tone emission we need, (i) positive growth rate $\Gamma_{NL} > 0$ and (ii) wave amplitude greater than the threshold amplitude. The oscillating field lines can change the threshold amplitude by influencing the magnetic field gradient through parameter $a$ (refer equation (6)) and the drifting ion species in the ring current can affect the growth rate (refer equation (4)) by modulating hot proton densities. The magnetic field line oscillations of few tens of nanotesla associated with the ULF waves (Motoba et al., 2013) indicate the 4-8% variations in the ambient magnetic field in the source region lying between L-shells 5-6. Moreover, the wavelength of ULF waves is very large (~ thousands kilometers), and these variations in the magnetic field exist over the larger spatial scales along the field line. These oscillations (i.e., moving back and forth with the ULF wave frequency) can change the curvature of magnetic field lines over larger spatial extent and can modify the value of $a$, thereby significantly modifying the threshold amplitude (see equation 8). Under such conditions the threshold amplitude required for the nonlinear growth of EMIC wave can be modulated considerably with the periods of the ULF waves. Thus, mechanisms proposed for the modulation of EMIC waves in the present work can affect the process of generation of EMIC rising tone emission in the source/generation region, and it is expected to see the modulation of EMIC rising tone emissions with the short and long periodicities as observed on 17 September 2011.

## 8. Summary and Conclusions

In this paper, we report the observation of EMIC waves in the ground magnetic records from the Indian Antarctic station Maitri. The EMIC wave event occurred on 17 September 2011, and its signatures were well recorded by the ICM operational at this station. The observed EMIC wave is characterized by the distinct appearance of rising tone emissions. We examined this event using the simultaneous ground PPM magnetic field, interplanetary solar wind parameters, and the GOES particle flux observations. The examination revealed many interesting features of EMIC rising tone emissions. On this day, the moderate increase in solar wind dynamic pressure (around 3.88 UT) was seen prior to the initiation of EMIC wave activity at the ground station Maitri around 4.7 UT (5.49 LT). The observation station Maitri was in dawn sector when the magnetosphere encountered this moderate shock. This moderate pressure pulse (or shock) could be the source for the observed EMIC wave activity. Earlier studies have reported that the dayside EMIC structured emissions are related to magnetospheric compression caused by an increase in the density or solar

wind pressure (Erlandson & Ukhorskiy, 2001; Halford et al., 2010; Usanova et al., 2008, 2012), which is in agreement with the present study.

The long periodicities reported here are relatively longer than the previously reported periodicities of Pc5 (1–10 mHz) waves (Fraser et al., 1992; Mursula et al., 2001). Our study indicates the modulation of high-frequency EMIC waves (Pc1) by low-frequency Pc5 geomagnetic pulsations, which is put forth using the spectral analysis of ICM data and PPM data from Indian Antarctic station Maitri. A similar mechanism was envisaged by Coroniti and Kennel (1970). It may be noted that both types of oscillations (toroidal and poloidal) can be excited due to the pressure imbalance at the magnetopause boundary (Sinha & Rajaram, 2003). Both of these oscillations can be the candidates for the low-frequency modulation of ion-cyclotron instability growth rate. However, the Pc5 pulsation analysis in this study does not differentiate whether the pulsations are toroidal or poloidal.

In the present study, we have proposed possible mechanism with a plausible theoretical explanation for both short- and long-period modulation of EMIC wave observed on 17 September 2011. The ring current particle drift frequency can provide a source for the observed modulation of EMIC waves through long-period oscillations. This is verified by the periodicity present in the *SYM-H* index, a measure of the ring current. When the solar wind pressure pulse (or shock) hits the Earth's magnetosphere the magnetospheric cavity oscillates due to sudden compression, which acts as a source for the field line oscillations at the $L$ shell corresponding to the generation region of EMIC waves. These field line oscillations can be a likely source for the observed short (Pc5) periodicity because such oscillations can modify the magnetic field gradient in the generation region of EMIC waves. Thus, changes in the hot ion density due to drifting ring current ions and the changes in the gradient of the magnetic field due to oscillating field line both can modify the growth rate and the threshold amplitude of wave required for the growth of self-sustaining EMIC rising tone emission. Hence, both these processes can be likely sources for the modulation of EMIC waves seen at Maitri on 17 September 2011. Earlier studies have reported that the periodicities for the field line oscillations at $L = 6.6$ lie in the range of 1–3 min for fundamental modes (Cummings et al., 1969).

We have incorporated a new method, based on the cross-correlation technique to determine the sweep rates of the observed discrete EMIC rising tones. The sweep rates of these emissions are found to be in the range of 0.44–1.9 mHz/s. These sweep rates are relatively low as compared to the past reports of sweep rates derived from the satellite observations of the EMIC wave (tens-hundreds mHz/s), which is attributed to the propagational effect. Our analysis reveals that the higher sweep rates are associated with the stronger EMIC emissions on the ground at subauroral latitudes, which is in agreement with the theoretical studies (Omura et al., 2010). It suggests that the theoretically proposed dependence of sweep rate on strength of EMIC wave in the generation region is retained even during the propagation of these waves to the ground.

We have also investigated the effect of the EMIC waves on the energetic electrons in the geosynchronous orbit. The observations of relativistic integral electron flux from GOES satellites suggest that the EMIC waves can cause precipitation of energetic electrons (0.8–2 MeV). In view of the potential role of EMIC rising tone emissions in the loss of MeV electrons from the radiation belts, the ICM observations from the Indian Antarctic station Maitri are crucial for deciphering inner magnetospheric dynamics.

**Acknowledgments**
This study was supported by Indo-JSPS project DSTIINT/JSPS/P-21 0/2015 and by JSPS KAKENHI Grant 17H06140. We thank N. Tsyganenko and his team for the magnetic field model available at http://ccmc.gsfc.nasa.gov/. We thank omniweb team for interplanetary data available at http://omniweb.gsfc.nasa.gov/ow_min.html and NASA NGDC team for IGRF model available at http://www.ngdc.noaa.gov/geomag-web. We are thankful to WDC Kyoto for SYM-H data. The ICM data will be made available on www.iigm.res.in on request at ashwini@iigs.iigm.res.in.

## References

Anderson, B. J., & Hamilton, D. C. (1993). Electromagnetic ion cyclotron waves stimulated by modest magnetospheric compressions. *Journal of Geophysical Research*, *98*(A7), 11,369–11,382. https://doi.org/10.1029/93JA00605

Baumjohann, W., Junginger, H., Haerendel, G., & Bauer, O. H. (1984). Resonant Alfvén waves excited by a sudden impulse. *Journal of Geophysical Research*, *89*(A5), 2765–2769. https://doi.org/10.1029/JA089iA05p02765

Baumjohann, W., & Treumann, R. (1997). *Basic Space Plasma Physics*. London: Imperial College Press.

Behera, J. K., Sinha, A. K., Vichare, G., Bhaskar, A., Honary, F., Rawat, R., & Singh, R. (2017). Enhancement and modulation of cosmic noise absorption in the afternoon sector at subauroral location (l = 5) during the recovery phase of 17 March 2015 geomagnetic storm. *Journal of Geophysical Research: Space Physics*, *122*, 9528–9544. https://doi.org/10.1002/2017JA024226

Behera, J. K., Sinha, A. K., Vichare, G., Kozyreva, O., Rawat, R., & Dhar, A. (2016). Dayside cosmic noise absorption at the equatorward boundary of auroral oval as observed from maitri, antarctica ($l$=5; cgm 62.45$^o$s, 55.45$^o$e). *Journal of Geophysical Research: Space Physics*, *121*, 3198–3211. https://doi.org/10.1002/2016JA022418

Boynton, R., Balikhin, M., Sibeck, D., Walker, S., Billings, S., & Ganushkina, N. (2016). Electron flux models for different energies at geostationary orbit. *Space Weather*, *14*, 846–860. https://doi.org/10.1002/2016SW001506

Briggs, B. H. (1984). The analysis of spaced sensor records by correlation techniques. In R. Vincent (Ed.), *Handbook for the Middle Atmosphere Program, Handbook for MAP* (Vol. 13, pp. 166–186). Special Committee for Solar-Terrestrial Physics Secretariat, University of Illinois, Urbana.

Chen, M. W., Roeder, J. L., Fennell, J. F., Lyons, L. R., Lambour, R. L., & Schulz, M. (1999). Proton ring current pitch angle distributions: Comparison of simulations with CRRES observations. *Journal of Geophysical Research*, *104*(A8), 17,379–17,389.

Chen, L., Thorne, R. M., Bortnik, J., & Zhang, X.-J. (2016). Nonresonant interactions of electromagnetic ion cyclotron waves with relativistic electrons. *Journal of Geophysical Research: Space Physics*, *121*, 9913–9925. https://doi.org/10.1002/2016JA022813

Coroniti, F., & Kennel, C. (1970). Electron precipitation pulsations. *Journal of Geophysical Research*, *75*(7), 1279–1289.

Cummings, W. D., O'Sullivan, R. J., & Coleman, P. J. (1969). Standing Alfvén waves in the magnetosphere. *Journal of Geophysical Research*, *74*(3), 778–793. https://doi.org/10.1029/JA074i003p00778

Daglis, I. A., Thorne, R. M., Baumjohann, W., & Orsini, S. (1999). The terrestrial ring current: Origin, formation, and decay. *Reviews of Geophysics*, *37*(4), 407–438.

Demekhov, A. (2007). Recent progress in understanding pc1 pearl formation. *Journal of Atmospheric and Solar-Terrestrial Physics*, *69*(14), 1609–1622.

Di Matteo, S., & Villante, U. (2018). The identification of waves at discrete frequencies at the geostationary orbit: The role of the data analysis techniques and the comparison with solar wind observations. *Journal of Geophysical Research: Space Physics*, *123*, 1953–1968. https://doi.org/10.1002/2017JA024922

Engavale, B., Jeeva, K., Nair, K. U., & Bhattacharyya, A. (2005). Solar flux dependence of coherence scales in scintillation patterns produced by ESF irregularities. *Annales Geophysicae*, *23*, 3261–3266. https://doi.org/10.5194/angeo-23-3261-2005

Engebretson, M. J., Peterson, W. K., Posch, J. L., Klatt, M. R., Anderson, B. J., Russell, C. T., et al. (2002). Observations of two types of Pc 1-2 pulsations in the outer dayside magnetosphere. *Journal of Geophysical Research*, *107*(A12), 1451. https://doi.org/10.1029/2001JA000198

Engebretson, M. J., Posch, J. L., Wygant, J. R., Kletzing, C. A., Lessard, M. R., Huang, C.-L., et al. (2015). Van Allen Probes, NOAA, goes, and ground observations of an intense EMIC wave event extending over 12 h in magnetic local time. *Journal of Geophysical Research: Space Physics*, *120*, 5465–5488. https://doi.org/10.1002/2015JA021227

Erlandson, R. E., & Ukhorskiy, A. J. (2001). Observations of electromagnetic ion cyclotron waves during geomagnetic storms: Wave occurrence and pitch angle scattering. *Journal of Geophysical Research*, *106*(A3), 3883–3895. https://doi.org/10.1029/2000JA000083

Fraser, B. J., Grew, R. S., Morley, S. K., Green, J. C., Singer, H. J., Loto'aniu, T. M., & Thomsen, M. F. (2010). Storm time observations of electromagnetic ion cyclotron waves at geosynchronous orbit: Goes results. *Journal of Geophysical Research*, *115*, A05208. https://doi.org/10.1029/2009JA014516

Fraser, B. J., Loto'aniu, T. M., & Singer, H. J. (2013). *Electromagnetic ion cyclotron waves in the magnetosphere* (pp. 195–212). Washington, DC: American Geophysical Union. https://doi.org/10.1029/169GM13

Fraser, B. J., Samson, J. C., Hu, Y. D., McPherron, R. L., & Russell, C. T. (1992). Electromagnetic ion cyclotron waves observed near the oxygen cyclotron frequency by ISEE 1 and 2. *Journal of Geophysical Research*, *97*(A3), 3063–3074. https://doi.org/10.1029/91JA02447

Fujita, S., Mizuta, T., Itonaga, M., Yoshikawa, A., & Nakata, H. (2001). Propagation property of transient MHD impulses in the magnetosphere-ionosphere system: The 2D model of the Pi2 pulsation. *Geophysical Research Letters*, *28*(11), 2161–2164. https://doi.org/10.1029/2000GL000108

Gilman, D. L., Fuglister, F. J., & Mitchell, J. M. Jr. (1963). On the power spectrum of red noise. *Journal of the Atmospheric Sciences*, *20*(2), 182–184.

Guo, Z., Wu, M., & Du, A. (2016). Generation of electromagnetic ion cyclotron waves in the near-earth magnetotail during dipolarization: Two-dimensional global hybrid simulation. *Physics of Plasmas*, *23*(4), 42902. https://doi.org/10.1063/1.4947567

Halford, A. J., Fraser, B. J., & Morley, S. K. (2010). EMIC wave activity during geomagnetic storm and nonstorm periods: CRRES results. *Journal of Geophysical Research*, *115*, A12248. https://doi.org/10.1029/2010JA015716

Johnson, J. R., & Cheng, C. (1999). Can ion cyclotron waves propagate to the ground? *Geophysical research letters*, *26*(6), 671–674.

Kakad, B., Omura, Y., Kakad, A., Upadhyay, A., & Sinha, A. K. (2018). Characteristics of subpacket structures in ground EMIC wave observations. *Journal of Geophysical Research: Space Physics*, *123*, 8358–8376. https://doi.org/10.1029/2018JA025473

Kangas, J., Guglielmi, A., & Pokhotelov, O. (1998). Morphology and physics of short-period magnetic pulsations. *Space Science Reviews*, *83*(3), 435–512. https://doi.org/10.1023/A:1005063911643

Kim, E.-H., & Johnson, J. R. (2016). Full-wave modeling of EMIC waves near the He+ gyrofrequency. *Geophysical Research Letters*, *43*, 13–21. https://doi.org/10.1002/2015GL066978

Kubota, Y., Omura, Y., & Summers, D. (2015). Relativistic electron precipitation induced by EMIC-triggered emissions in a dipole magnetosphere. *Journal of Geophysical Research: Space Physics*, *120*, 4384–4399. https://doi.org/10.1002/2015JA021017

Lorentzen, K. R., McCarthy, M. P., Parks, G. K., Foat, J. E., Millan, R. M., Smith, D. M., et al. (2000). Precipitation of relativistic electrons by interaction with electromagnetic ion cyclotron waves. *Journal of Geophysical Research*, *105*(A3), 5381–5389. https://doi.org/10.1029/1999JA000283

Loto'Aniu, T., Fraser, B., & Waters, C. (2009). The modulation of electromagnetic ion cyclotron waves by Pc 5 ULF waves. *Annales Geophysicae*, *27*, 121–130. https://doi.org/10.5194/angeo-27-121-2009

Manu, S., Rawat, R., Sinha, A. K., Gurubaran, S., & Jeeva, K. (2015). Schumann resonances observed at Maitri, Antarctica: Diurnal variation and its interpretation in terms of global thunderstorm activity. *Current Science*, *109*(4), 784–790. https://doi.org/10.18520/cs/v109/i4/784-790

Menk, F. W. (2011). *Magnetospheric ULF Waves: A Review* (pp. 223–256). Dordrecht: Springer Netherlands. https://doi.org/10.1007/978-94-007-0501-2_13

Meredith, N. P., Thorne, R. M., Horne, R. B., Summers, D., Fraser, B. J., & Anderson, R. R. (2003). Statistical analysis of relativistic electron energies for cyclotron resonance with EMIC waves observed on CRRES. *Journal of Geophysical Research*, *108*(A6), 1250. https://doi.org/10.1029/2002JA009700

Min, K., Lee, J., Keika, K., & Li, W. (2012). Global distribution of EMIC waves derived from THEMIS observations. *Journal of Geophysical Research*, *117*, A05219. https://doi.org/10.1029/2012JA017515

Motoba, T., Takahashi, K., Gjerloev, J., Ohtani, S., & Milling, D. (2013). The role of compressional Pc5 pulsations in modulating precipitation of energetic electrons. *Journal of Geophysical Research: Space Physics*, *118*, 7728–7739. https://doi.org/10.1002/2013JA018912

Mursula, K. (2007). Satellite observations of Pc 1 pearl waves: The changing paradigm. *Journal of Atmospheric and Solar-Terrestrial Physics*, *69*(14), 1623–1634. https://doi.org/10.1016/j.jastp.2007.02.013, pc1 Pearl Waves: Discovery, Morphology and Physics.

Mursula, K., Brysy, T., Niskala, K., & Russell, C. T. (2001). Pc1 pearls revisited: Structured electromagnetic ion cyclotron waves on Polar satellite and on ground. *Journal of Geophysical Research*, *106*(A12), 29,543–29,553. https://doi.org/10.1029/2000JA003044

Nakamura, S., Omura, Y., Machida, S., Shoji, M., Nosé, M., & Angelopoulos, V. (2014). Electromagnetic ion cyclotron rising tone emissions observed by THEMIS probes outside the plasmapause. *Journal of Geophysical Research: Space Physics*, *119*, 1874–1886. https://doi.org/10.1002/2013JA019146

Nomura, R., Shiokawa, K., Omura, Y., Ebihara, Y., Miyoshi, Y., Sakaguchi, K., et al. (2016). Pulsating proton aurora caused by rising tone Pc1 waves. *Journal of Geophysical Research: Space Physics*, *121*, 1608–1618. https://doi.org/10.1002/2015JA021681

Omura, Y., Pickett, J., Grison, B., Santolik, O., Dandouras, I., Engebretson, M., et al. (2010). Theory and observation of electromagnetic ion cyclotron triggered emissions in the magnetosphere. *Journal of Geophysical Research*, *115*, A07234. https://doi.org/10.1029/2010JA015300

Omura, Y., & Zhao, Q. (2012). Nonlinear pitch angle scattering of relativistic electrons by EMIC waves in the inner magnetosphere. *Journal of Geophysical Research*, *117*, A08227. https://doi.org/10.1029/2012JA017943

Omura, Y., & Zhao, Q. (2013). Relativistic electron microbursts due to nonlinear pitch angle scattering by EMIC triggered emissions. *Journal of Geophysical Research: Space Physics*, *118*, 5008–5020. https://doi.org/10.1002/jgra.50477

Pickett, J. S., Grison, B., Omura, Y., Engebretson, M. J., Dandouras, I., Masson, A., et al. (2010). Cluster observations of EMIC triggered emissions in association with Pc1 waves near earth's plasmapause. *Geophysical Research Letters*, *37*, L09104. https://doi.org/10.1029/2010GL042648

Rasinkangas, R., & Mursula, K. (1998). Modulation of magnetospheric EMIC waves by Pc 3 pulsations of upstream origin. *Geophysical research letters*, *25*(6), 869–872.

Rasinkangas, R., Mursula, K., Kremser, G., Singer, H., Fraser, B., Korth, A., & Hughes, W. (1994). Simultaneous occurrence of Pc 5 and Pc 1 pulsations in the dawnside magnetosphere: CRRES observations. *Geophysical Monograph-American Geophysical Union*, *81*, 417–424.

Remya, B., Sibeck, D., Halford, A., Murphy, K., Reeves, G., Singer, H., et al. (2018). Ion injection triggered EMIC waves in the Earth's magnetosphere. *Journal of Geophysical Research: Space Physics*, *123*, 4921–4938. https://doi.org/10.1029/2018JA025354

Remya, B., Tsurutani, B. T., Reddy, R. V., Lakhina, G. S., & Hajra, R. (2015). Electromagnetic cyclotron waves in the dayside subsolar outer magnetosphere generated by enhanced solar wind pressure: EMIC wave coherency. *Journal of Geophysical Research: Space Physics*, *120*, 7536–7551. https://doi.org/10.1002/2015JA021327

Sakaguchi, K., Kasahara, Y., Shoji, M., Omura, Y., Miyoshi, Y., Nagatsuma, T., et al. (2013). Akebono observations of EMIC waves in the slot region of the radiation belts. *Geophysical Research Letters*, *40*, 5587–5591. https://doi.org/10.1002/2013GL058258

Sakaguchi, K., Shiokawa, K., Ieda, A., Miyoshi, Y., Otsuka, Y., Ogawa, T., et al. (2007). Simultaneous ground and satellite observations of an isolated proton arc at subauroral latitudes. *Journal of Geophysical Research*, *112*, A04202. https://doi.org/10.1029/2006JA012135

Sandanger, M., Sraas, F., Aarsnes, K., Oksavik, K., & Evans, D. S. (2007). Loss of relativistic electrons: Evidence for pitch angle scattering by electromagnetic ion cyclotron waves excited by unstable ring current protons. *Journal of Geophysical Research*, *112*, A12213. https://doi.org/10.1029/2006JA012138

Schulz, M., & Mudelsee, M. (2002). REDFIT: Estimating red-noise spectra directly from unevenly spaced paleoclimatic time series. *Computers & Geosciences*, *28*(3), 421–426.

Shoji, M., & Omura, Y. (2011). Simulation of electromagnetic ion cyclotron triggered emissions in the Earth's inner magnetosphere. *Journal of Geophysical Research*, *116*, A05212. https://doi.org/10.1029/2010JA016351

Shoji, M., & Omura, Y. (2014). Spectrum characteristics of electromagnetic ion cyclotron triggered emissions and associated energetic proton dynamics. *Journal of Geophysical Research: Space Physics*, *119*, 3480–3489. https://doi.org/10.1002/2013JA019695

Shoji, M., Omura, Y., Grison, B., Pickett, J., Dandouras, I., & Engebretson, M. (2011). Electromagnetic ion cyclotron waves in the helium branch induced by multiple electromagnetic ion cyclotron triggered emissions. *Geophysical Research Letters*, *38*, L17102. https://doi.org/10.1029/2011GL048427

Singh, A. K., Sinha, A. K., Rajaram, R., & Pathan, B. M. (2012). Storm-time longitudinally propagating asymmetric modes at low latitudes. *Annales Geophysicae*, *30*(1), 131–141. https://doi.org/10.5194/angeo-30-131-2012

Sinha, A. K., & Rajaram, R. (2003). Dominance of toroidal oscillations in dawn/dusk sectors: A consequence of solar wind pressure variation, Earth. *Planets and Space*, *55*(2), 93–104. https://doi.org/10.1186/BF03351736

Summers, D., & Ma, C.-y. (2000). A model for generating relativistic electrons in the Earth's inner magnetosphere based on gyroresonant wave-particle interactions. *Journal of Geophysical Research*, *105*(A2), 2625–2639. https://doi.org/10.1029/1999JA900444

Summers, D., & Thorne, R. M. (2003). Relativistic electron pitch-angle scattering by electromagnetic ion cyclotron waves during geomagnetic storms. *Journal of Geophysical Research*, *108*(A4), 1143. https://doi.org/10.1029/2002JA009489

Tetrick, S., Engebretson, M., Posch, J., Olson, C., Smith, C., Denton, R., et al. (2017). Location of intense electromagnetic ion cyclotron (EMIC) wave events relative to the plasmapause: Van Allen Probes observations. *Journal of Geophysical Research: Space Physics*, *122*, 4064–4088. https://doi.org/10.1002/2016JA023392

Usanova, M. E., Mann, I. R., Bortnik, J., Shao, L., & Angelopoulos, V. (2012). THEMIS observations of electromagnetic ion cyclotron wave occurrence: Dependence on AE, SYM-H, and solar wind dynamic pressure. *Journal of Geophysical Research*, *117*, A10218. https://doi.org/10.1029/2012JA018049

Usanova, M. E., Mann, I. R., Kale, Z. C., Rae, I. J., Sydora, R. D., Sandanger, M., et al. (2010). Conjugate ground and multisatellite observations of compression-related EMIC pc1 waves and associated proton precipitation. *Journal of Geophysical Research*, *115*, A07208. https://doi.org/10.1029/2009JA014935

Usanova, M., Mann, I., Rae, I., Kale, Z., Angelopoulos, V., Bonnell, J., et al. (2008). Multipoint observations of magnetospheric compression-related EMIC Pc1 waves by THEMIS and CARISMA. *Geophysical Research Letters*, *35*, L17S25. https://doi.org/10.1029/2008GL034458

Welch, P. (1967). The use of fast fourier transform for the estimation of power spectra: A method based on time averaging over short, modified periodograms. *IEEE Transactions on Audio and Electroacoustics*, *15*(2), 70–73.

Yahnin, A. G., Yahnina, T. A., Frey, H. U., Bsinger, T., & Manninen, J. (2009). Proton aurora related to intervals of pulsations of diminishing periods. *Journal of Geophysical Research*, *114*, A12215. https://doi.org/10.1029/2009JA014670

Yahnina, T. A., & Yahnin, A. G. (2014). Proton precipitation to the equator of the isotropic boundary during the geomagnetic storm on november 20–29, 2003. *Cosmic Research*, *52*(1), 79–85. https://doi.org/10.1134/S0010952514010092

Yue, C., Bortnik, J., Li, W., Ma, Q., Gkioulidou, M., Reeves, G. D., et al. (2018). The composition of plasma inside geostationary orbit based on Van Allen Probes observations. *Journal of Geophysical Research: Space Physics*, *123*, 6478–6493. https://doi.org/10.1029/2018JA025344

Zhang, X., Zong, Q.-G., Wang, Y., Zhang, H., Xie, L., Fu, S., et al. (2010). ULF waves excited by negative/positive solar wind dynamic pressure impulses at geosynchronous orbit. *Journal of Geophysical Research*, *115*, A10221. https://doi.org/10.1029/2009JA015016

Zhao, H., Li, X., Baker, D., Fennell, J., Blake, J., Larsen, B. A., et al. (2015). The evolution of ring current ion energy density and energy content during geomagnetic storms based on Van Allen Probes measurements. *Journal of Geophysical Research: Space Physics*, *120*, 7493–7511. https://doi.org/10.1002/2015JA021533